

https://dspace.org/

Development of carbon nanotube/platinum electrocatalytic electrodes for proton exchange membrane fuel cell

Afolabi, Ayo Samuel

2010-03-10T07:10:24Z
http://hdl.handle.net/10539/7652

Downloaded from a DSpace repository. https://dspace.org/

5.0 ELECTROLYTIC ELECTRODES AND MEA PERFORMANCES

This chapter presents the discussion of the results obtained from the preparation of various loadings of Pt–CNT catalyst, characterization and electrochemical analysis of the catalyst. The casting of the catalyst electrodes, fabrication of the membrane electrode assembly (MEA) using the electrocatalytic electrodes and sulphonated membrane, testing and analysis of this unit in a PEM fuel cell test station are also reported in this chapter.

5.1 Preparation of Pt–CNT Catalysts

5.1.1 Functionalization of CNTs

Figure 5.1 shows the Fourier transform infrared (FT IR) spectrum of the functionalized CNT sample. This was used to analyze the changes in the surface chemical bonding and structures in the frequency range of 4000 – 500 cm^{-1}. It can be observed that the peak at 1670 cm^{-1} shows the beginning of the carbonyl stretch which terminates at 1820 cm^{-1} on the functionalized CNT, while a broad stretch between 3200 and 3600 cm^{-1} represents OH functional group.

It is suspected that free oxygen radicals were produced during the acid treatment of CNT samples. These free radicals might have resulted into oxygen atoms which might have combined with carbon atoms to form the >C = O group that was introduced into the CNT surface. This C = O group combined with a –OH group at the same carbon atom to form –COOH group (Shaffer *et al.*, 1998; Jia *et al*., 1999; Li *et al.*, 2002; Zhou *et al*., 2007).

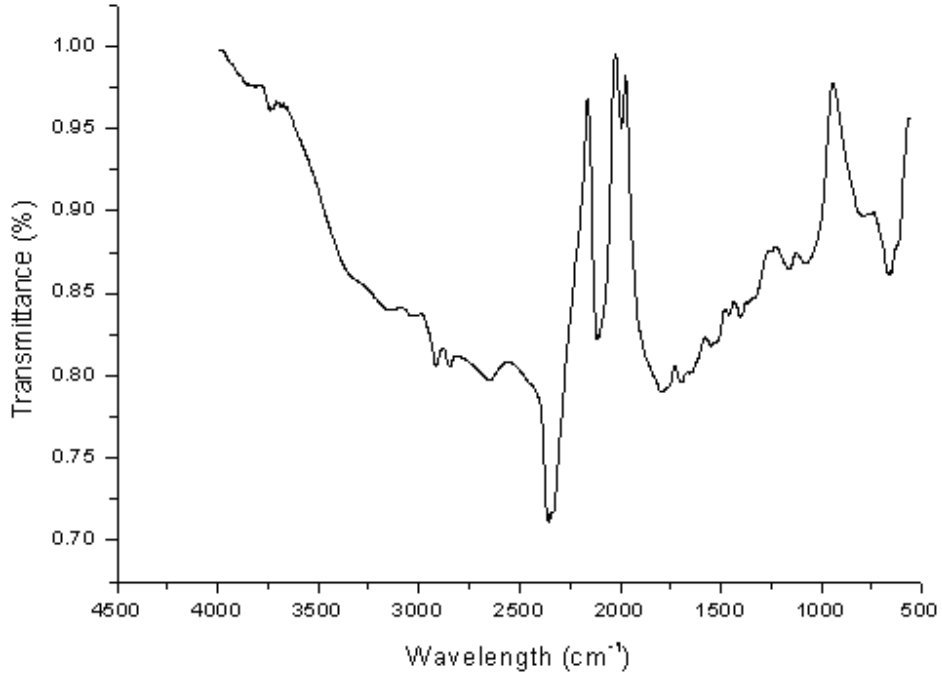

Figure 5.1: FT IR spectra of functionalized CNT sample

5.2 Platinum Loading on the CNT

The amount of platinum loaded on the CNT substrate was determined by using a spectrophotometric method. A calibration of absorbance versus concentration profile was obtained by preparing various concentrations of K_2PtCl_4. The absorbance values of these standard solutions were measured using a UV spectrophotometer at constant wavelength of Pt at λ = 325 nm (Prado–Burguete *et al*., 1989). These values were used to plot the absorbance profile shown in Figure 5.2. It is observed from the profile that a maximum absorbance is obtained when the concentration of K_2PtCl_4 is 0.35 g/cm^3. This

concentration value was chosen as reference to prepare the 10, 20, 30, 40 and 50 wt% loadings of platinum on one gram of the functionalized CNTs.

Thus: For 10 wt% Pt catalyst; $\frac{10}{100}$ X $0.35 = 0.035$ g/cm^3.

This means that 0.035 g/cm^3 of platinum ions will be required to prepare 10 wt% Pt–CNT catalyst on one gram of CNT support (Appendix II). Multiples of these standard solutions were employed to prepare catalyst samples using 2, 3, 4, and 5 gram on the purified CNTs.

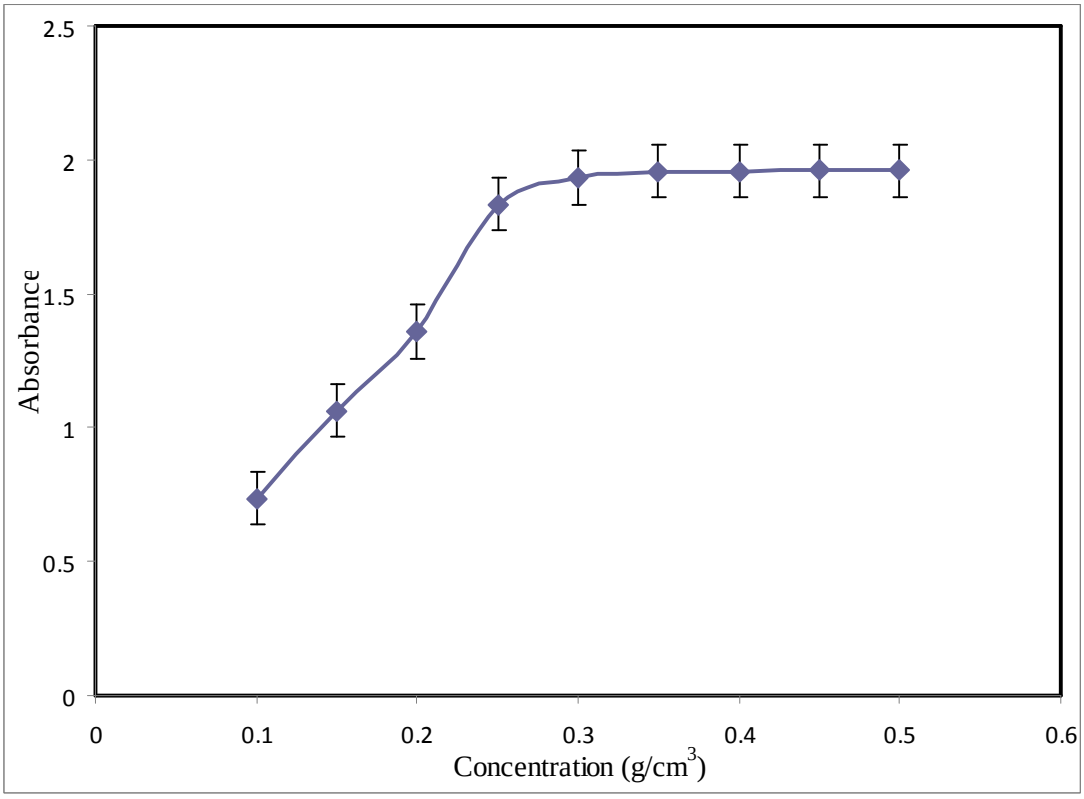

Figure 5.2: Calibration curve for absorbance profile of Pt in CNT (standard deviation = 0.7665)

A specified quantity of CNT (usually 1 g) was ultrasonicated with a known concentration of the platinum precursor (K_2PtCl_4) for specific period of time. The mixture was filtered and the concentration of the filtrate was measured and correlated with the data in the absorbance profile. The difference in concentration represents the amount of platinum deposited on the CNT. This amount was further confirmed by the TGA analyses shown in Figure 5.10 of the purified CNT and a Pt–CNT catalyst sample. The drops in the two curves are conspicuous and their difference confirms the amount of the platinum impregnated on the CNT. Using the profile, the effect of stirring time on the amount of Pt adsorbed on various CNTs at 0.35 g/cm^3 concentration of K_2PtCl_4 was investigated and the results are presented in Figure 5.3.

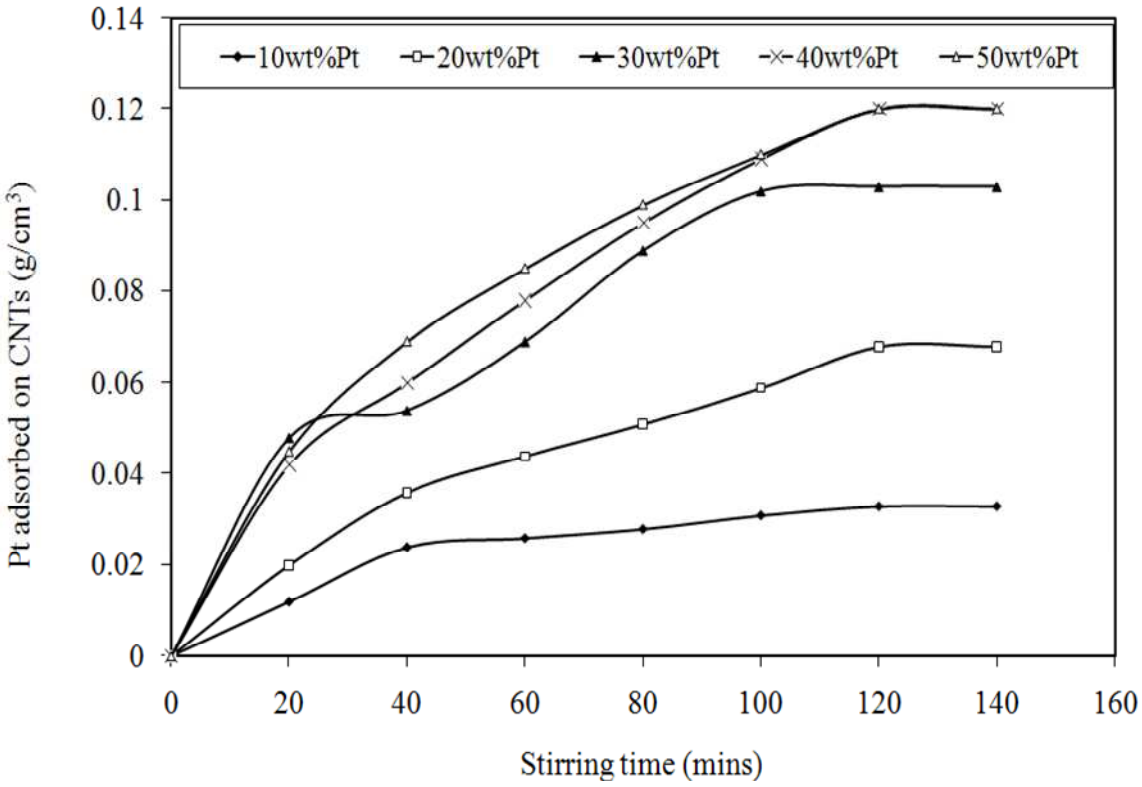

Figure 5.3: Effect of stirring time on Pt adsorbed on CNTs

It is seen from the figure that increase in stirring time produces more Pt particles adsorbed on the carbon material for all the loadings of the catalyst. As expected, the Pt content in the CNT samples increases with increase in loading of the catalysts. A maximum adsorption of all the catalyst samples is achieved at 120 minutes stirring time but the 40wt% and 50wt% catalyst samples have the same maximum adsorbtion at the same time stiring time of 120 minutes. This indicates that at this time, the specific quantity of CNT employed in the preparation of the catalyst has been saturated and can no longer adsorb more Pt particles. The total percentage of Pt adsorbed per loading is calculated using the equation;

$$\% \text{ Pt adsorbed} = \frac{Co - Ce}{Co} \times 100\% \quad \text{(Zheng } et\ al.\text{, 2008)} \qquad (5.1)$$

where Co and Ce are the respective initial and final concentrations of the platinic salt.

Using the optimum time of 120 minutes where a maximum Pt particles were adsorbed on the CNTs, the effect of the temperature on the adsorption of Pt was investigated and the results obtained are plotted in Figure 5.4. From the figure, it is observed that temperature has an effect on the Pt adsorbed on this materials. A maximum of 97% of the total Pt was loaded on the 10wt% catalyst sample in maximum stirring time of 120 minutes at the temperature of 100°C, while the 20 – 40wt% catalyst samples have 99% of the total platinum adsorbed on the carbon material at these same conditions. The 50wt% catalyst has the least Pt adsorbtion of 70%. The high content of Pt adsorbtion is traceable to the increase in temperature of the mixture which brings about an increase in the rate of

adsorption of the Pt precursor at the fixed stirring time of 120 minutes. It is therefore appropriate to say that increase in temperature increases the amount of the Pt particles adsorbed on the CNT within the temperature range studied in this work (25 – 100°C).

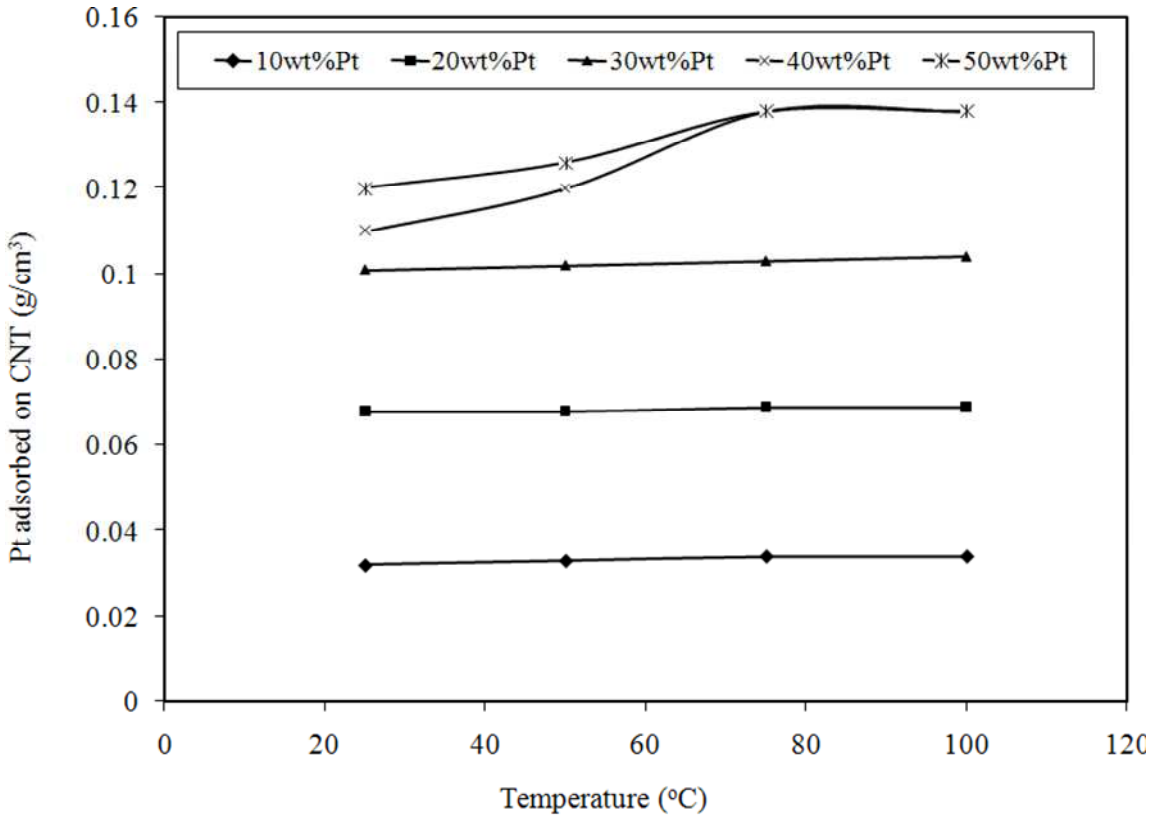

Figure 5.4: Effect of temperature on Pt adsorbed on CNTs

Therefore, using these optimum conditions of 120 minutes and 80°C, 10 – 40wt% Pt–CNT catalysts were prepared for the electrocatalytic electrodes and for subsequent characterisation and analyses of the Pt–CNT material. The 50wt% Pt–CNT catalyst was not chosen because the Pt loadings on the 50wt% and 40wt% catalysts are almost the

same. The results of the characterisations carried out on these catalysts are discussed in section 5.3.

5.3 Characterisation of Pt–CNT Catalysts

5.3.1 TEM images of Pt–CNT catalysts

A high magnification TEM study as described in sub–section 3.1.3 was used to investigate the surface morphology and structure of the catalyst samples. Figures 5.5 and 5.6 show the TEM images of CNT loaded with platinum particles of 10, 20, 30 and 40 wt% Pt respectively. The tiny dark spots on the matrices of CNT are platinum particles as confirmed by EDX (Figure 5.7) and it is evident from these figures that these particles are well–dispersed and homogeneously anchored within the surface of the CNTs. The bar graphs located on the right of the TEM images show the size distribution of the Pt particles, obtained by randomly measuring the sizes of about 80 particles per surface in the magnified TEM images. These TEM images show the distribution and particle size of the platinum nanoparticles on the CNTs. It can be seen that these particles are adsorbed to the surface of the CNTs. These surfaces have been activated and functionalized by the pre–treatment of the carbon nanotubes during purification. The treatment of CNTs with a mixture of concentrated nitric and sulphuric acids did not only purify these carbon nanomaterials but also resulted in the formation of carbonyl and hydroxyl groups (Mawhinney *et al.,* 2000; Hu *et al*., 2001; Yu and Brus, 2000; Kuznetsova *et al*., 2001; Kukovecz *et al*., 2002) which acted as anchoring sites and induced the impregnation of platinum nanoparticles (Gomez de la Fuente *et al.,* 2006). The formation of these

nanoparticles on the functionalized surfaces of CNTs involves nucleation, growth, coagulation and flocculation, but the presence of the CNT might have interrupted the nucleation during the platinum crystallization process which might have prevented the coagulation and flocculation processes. This further explains the reason for deposition of fine platinum nanoparticles within the carbon nanotube networks.

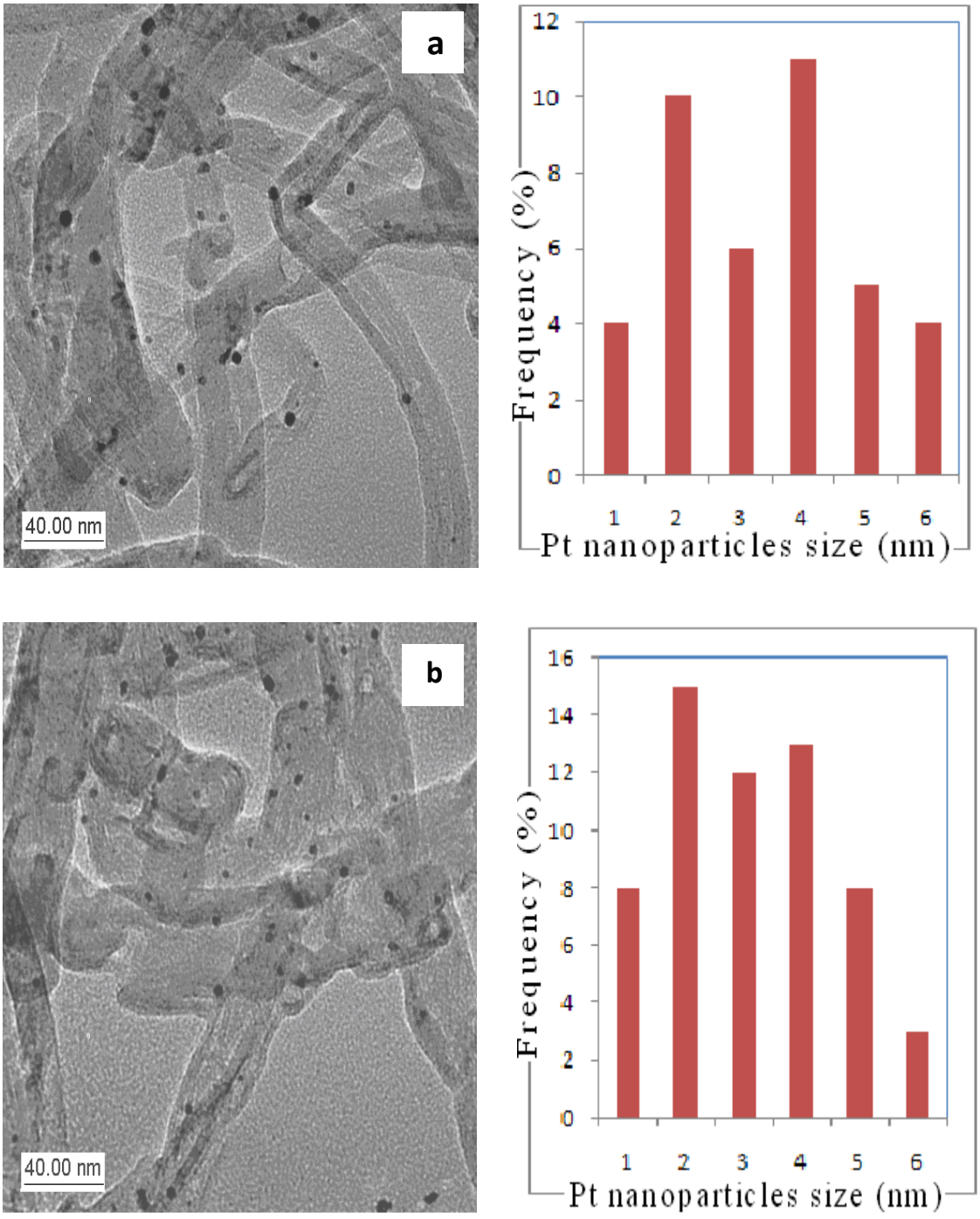

Figure 5.5: TEM images of Pt–CNT catalysts with (a) 10 wt% and (b) 20 wt% loading of platinum. The particle size distributions of metallic Pt in various loadings of the catalysts are located beside the TEM images.

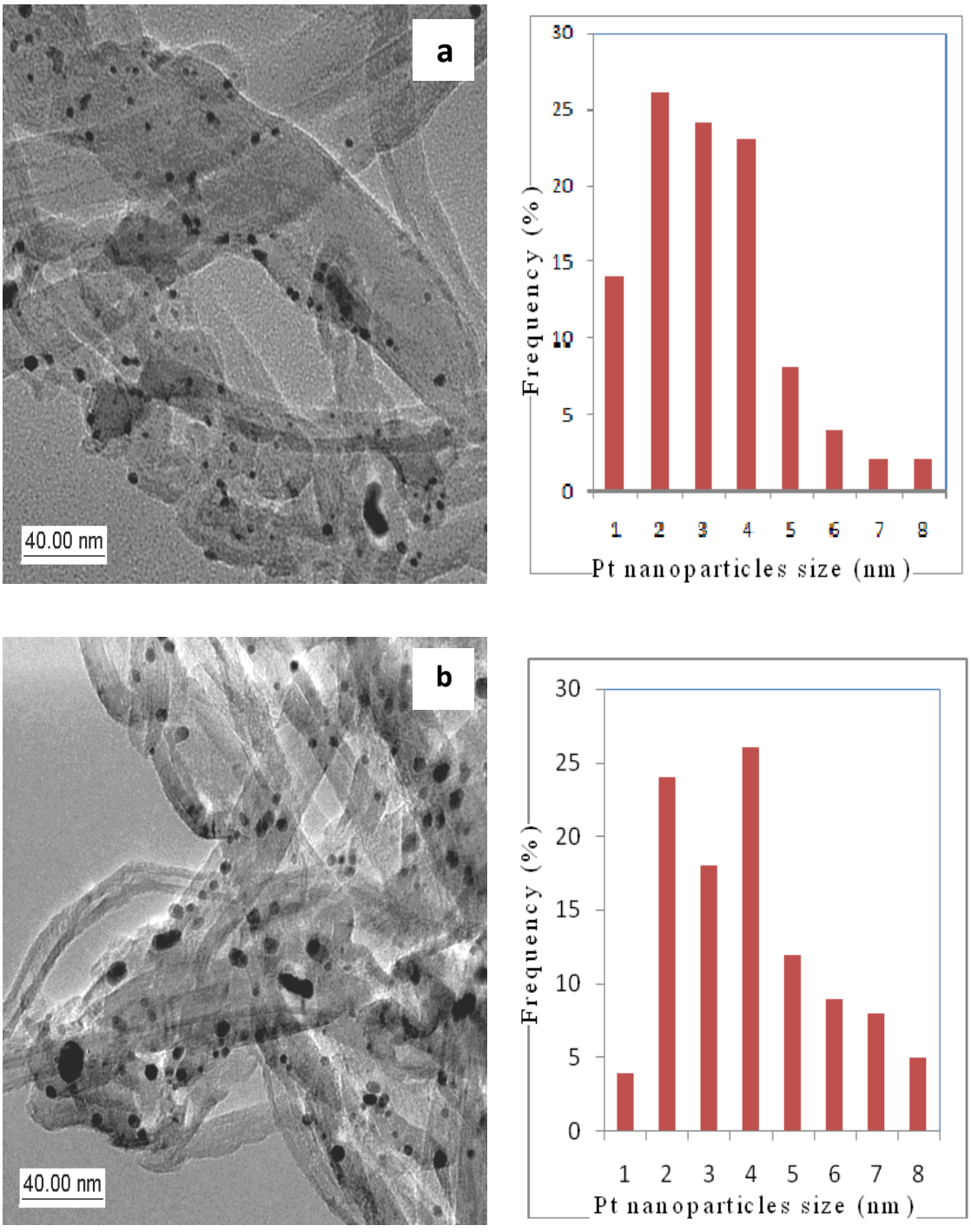

Figure 5.6: TEM images of Pt–CNT catalysts with (a) 30 wt% and (b) 40 wt% loading of platinum. The particle size distributions of metallic Pt in various loadings of the catalysts are located beside the TEM images.

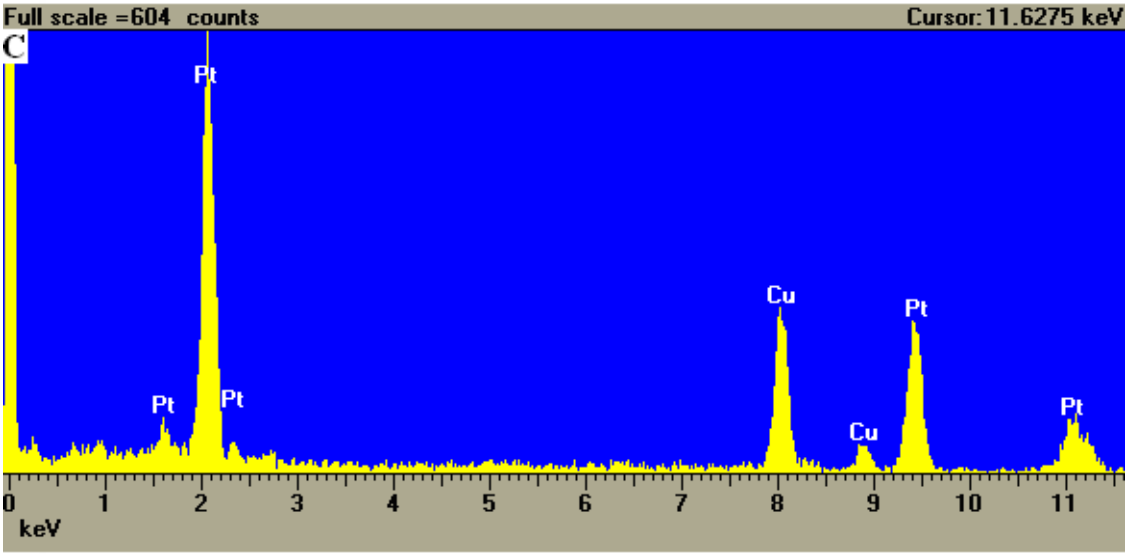

Figure 5.7: EDX analysis of the Pt–CNT catalyst sample confirming the presence of Pt.

Figure 5.8 shows the platinum particles distribution within various loadings of the catalysts as estimated from the TEM images. It can be seen that these metal particles increase with increase in loadings of the catalysts. A closer look at the TEM images shows that the catalyst samples with 30 and 40 wt% loadings have bigger metal particles than the remaining loadings of the catalyst prepared under the same conditions. This may be attributed to the fact that higher concentrations of the Pt precursor salt were used to prepare higher loadings of the catalyst on the same quantity (1 g) of CNT support. It is believed that the higher quantity of the carbon support will be required to match the high concentrations of the platinic salt to produce even distribution of these metal particles on the support. The above will also require more ethyl glycol whereas equal quantity of this reagent was used during the preparation of all the catalysts.

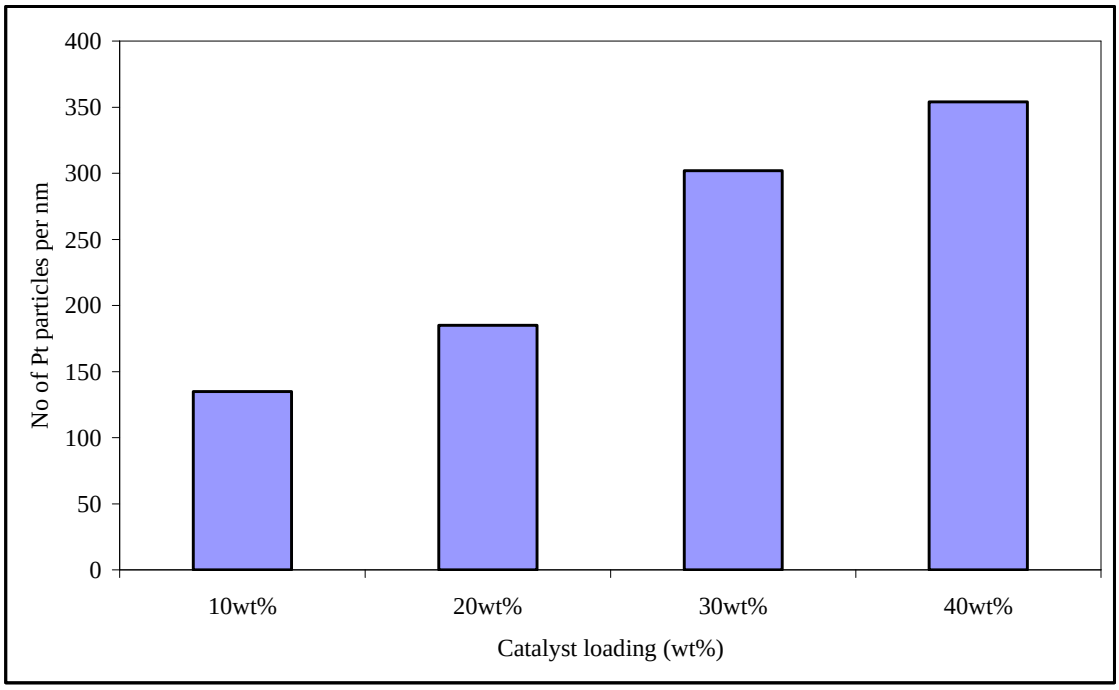

Figure 5.8: Histograms for the Pt distribution in various loadings of the catalysts as shown in the TEM images.

These metal particles attached to the activated and/or functionalized surfaces of the carbon nanotubes produce the catalysts. The size of these metal particles range from 1 nm to 8 nm which is close to the average size values obtained in the findings of (Li *et al.*, 2004a; Chai *et al.*, 2004; Matsumoto *et al.*, 2004; Rajalakshmi *et al.*, 2005; Tsai *et al.*, 2006). The particle sizes of these metals are within the nano–range and their ramdom distribution in the CNTs network make the resultant Pt–CNT catalyst a viable prospect as an electrocatalyst for hydrogen oxidation and oxygen reduction reactions in a typical PEM fuel cell reaction (Ciureanu and Wang, 1999; Lordi *et al.*, 2001; Li *et al.*, 2002a; Liu *et al.*, 2002; Joo *et al*. 2006; Kotobuki *et al.*, 2006; Liu *et al.*, 2007).

Ethyl glycol which functioned as the stabilizing surfactant is believed to be favourable for the production of small metal particles and also acted as a reducing agent during the preparation of the CNT–Pt nanocatalyst. This reagent is believed to be responsible for the reduction of the platinum ions to platinum atoms during stirring of ethyl glycol with the platinum precursor salt. Authors such as Li *et al*. (2003), Matsumoto *et al.* (2004), Li *et al.* (2005), Chen *et al*. (2006), Jeng *et al.* (2006) and Xie *et al.* (2006) have employed the use of this reagent as a reducing agent while gaseous phase reducing agents notably hydrogen have been used by other researchers (Carmo *et al.*, 2005; Zheng *et al.,* 2006; Onoe *et al.,* 2007).

These Pt–CNT materials were heat–treated at 300°C for sixteen hours followed by slow annealing in static air for another two hours while the temperature was reduced to about 50°C. This form of heat treatment is an important and necessary step in the preparation of the catalyst because it has a significant impact on the metal particle size and size distribution, particle surface morphology, and metal distribution on the support (Han *et al*., 2007). The calcination or thermal treatment, removed the volatile compounds contained in the catalyst and removed the undesirable impurities resulting from the early preparation stages, to allow a uniform dispersion and stable distribution of these metal particles on the support, and therefore improves the electrocatalytic activity of the synthesized catalyst (Hinds, 2005). The heat treatment period is also crucial to create the particle distribution of the Pt nanoparticles observed on the CNT support. Although this factor was not studied in this work, it is believed that a fast heating rate and short heating

period might cause agglomeration of the Pt particles thereby preventing their even distribution on the support (Hinds, 2005).

5.3.2 XRD analysis of Pt–CNT catalysts

Figure 5.9 reveals the XRD pattern which shows the diffraction peaks at $2\theta = 26.5^{o}C$ that can be attributed to the graphitic (002) planes of the CNT support, while other peaks at 39.74^{o}, 46.13^{o} and 67.29^{o} identify the characteristic face centred cubic (fcc) structure of crystalline platinum planes of Pt at (111), Pt (200), Pt (220), respectively. This indicates that Pt nanoparticles are composed of pure crystalline Pt since no other peaks are observed in the XRD patterns as also observed by other authors (Zhao *et al.,* 2006; Onoe *et al.,* 2007; Yang *et al.,* 2007; Nataranjan and Hamelin, 2007). Such spectra indicate that the platinum precursor employed (K_2PtCl_4) in this work has been reduced to metallic platinum as confirmed in the work of Bayrakceken *et al.* (2007). The lattice parameters of platinum as revealed by XRD is 3.9240 Å which corresponds to the value specified by McClune (1981).

Using Scherrer's formula: $D = \frac{\kappa\lambda}{\beta Cos\theta}$ 5.2

where D = the average crystalline size of the platinum particles

K = the Scherrer constant = 0.89

λ = the wavelength of X–ray radiation which is equal to 1.54051Å (0.154051nm).

β = the full width at half – maximum (FWHM) of the (111, 200, etc) diffraction line.

θ = the Bragg angle measured in radians at the position of platinum peaks (Cullity, 1984; Kinoshita, 1988; Kim and Park, 2006; Nataranjan and Hamelin, 2007; Yang *et al.* 2007), the average spherical size of the crystalline Pt particle was calculated from the major diffraction peak Pt (111) and it is found that the Pt nanoparticles on the CNTs have an average size of 2.3 nm which is close to the average size obtained in the TEM images of 10 and 20 wt% catalyst samples.

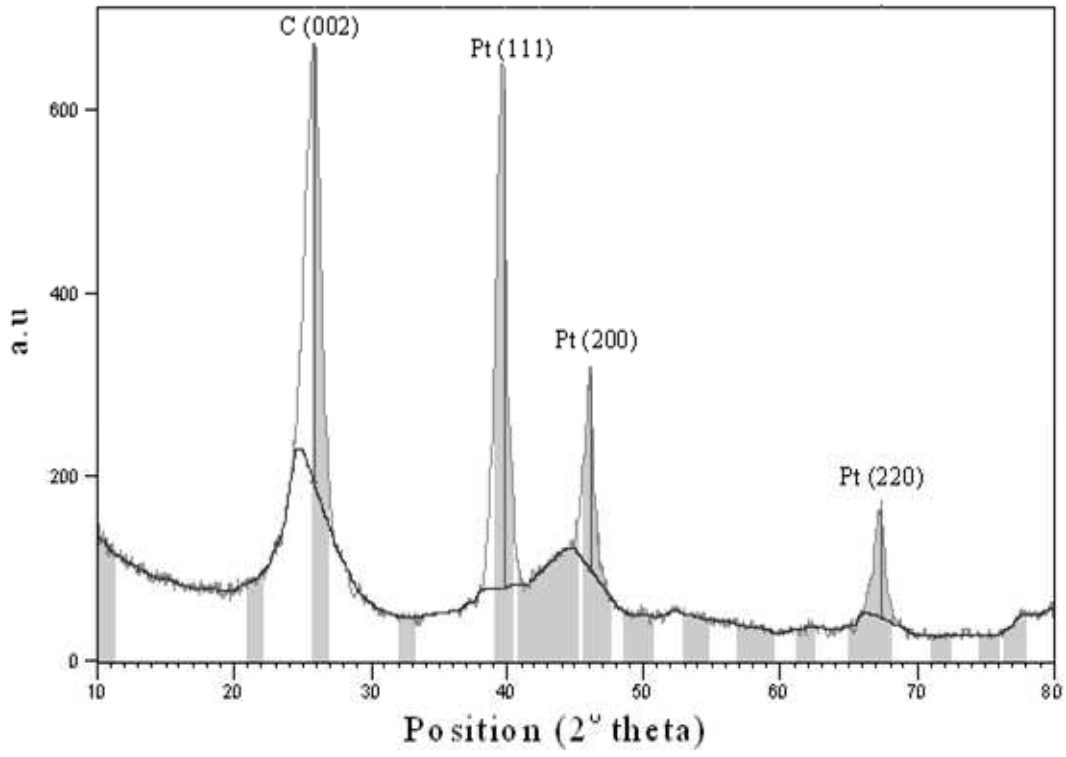

Figure 5.9: XRD pattern of Pt–CNT catalyst sample

It is well known that the catalytic activity of metal particles is strongly dependent on their particle size and distribution. The smaller the catalyst particles, the higher are their catalytic activity. The analyses of the TEM and XRD of the CNT-Pt samples show that the particles are small and well distributed on the surface of the CNTs.

5.3.3 BET analysis of the Pt–CNT catalysts

Table 5.1 shows the BET comparison of the purified CNT and various Pt–CNT catalysts. It is seen that the pore volumes decrease with increase in the amount of Pt. particles in the catalyst samples. This indicates that higher content of Pt reduced the pore size in the CNT samples. The surface areas of the catalyst samples also reduced with increase in Pt content in the CNT.

Table 5.1: BET analysis of CNT and Pt–CNT catalyst samples.

Sample	*Surface area (m^2/g)*	*Pore volume (cm^3/g)*
Purified CNT	118	0.37
10 wt% CNT–Pt	109	0.35
20 wt% CNT–Pt	92	0.33
30 wt% CNT–Pt	79	0.25
40 wt% CNT–Pt	65	0.21

5.3.4 TGA analysis of the Pt–CNT catalysts

The TGA curve (Figure 5.9) for a purified CNT sample shows that about 96% of this material decomposed in air at about 500°C. This is the characteristic curve of a crystalline carbon confirming very little or no presence of both metallic impurities and amorphous carbon. On the other hand, the curve for Pt–CNT catalyst shows a drop at about 400°C which is in the range of the reducing temperature of platinum (Burbidge, 1977). The difference between these two curves shows the exact content of platinum impregnated on the CNTs. This confirms the presence of metallic inclusion which is the platinum nanoparticles that had been deposited onto the CNTs.

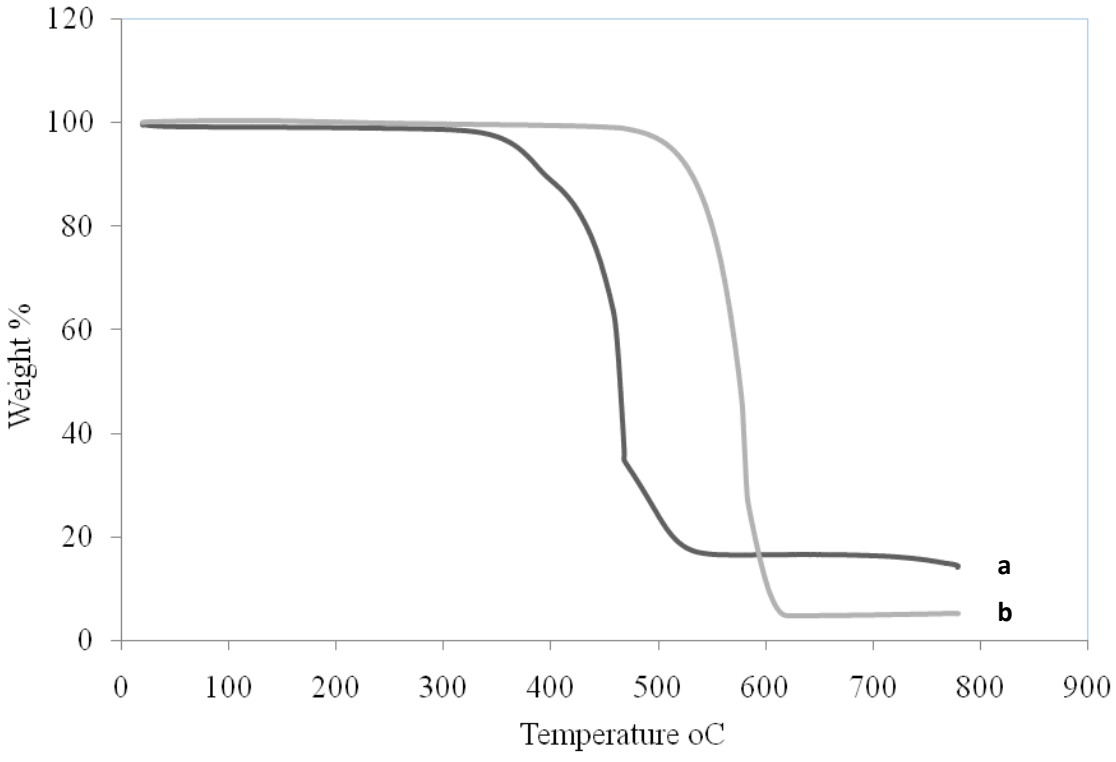

Figure 5.10: TGA curves of (a) Pt–CNT catalyst and (b) purified CNT samples showing 10 wt% Pt loading.

The TGA curve shown in Figure 5.10 could also be used to determine the stability and the purity of both the CNT and catalyst samples. The purified CNT sample was stable up till about 500°C. The Pt–CNT catalyst sample on the other hand, shows thermal stability up to about 400°C which was due to the presence of platinum particles in the CNT which catalyzed the decomposition of the CNT at such a lower temperature. This also gives an indication that the catalyst sample can withstand a working temperature of up to 400°C which is far higher than the working temperature of a PEM fuel cell (about 90°C).

5.3.5 Electrochemical measurements of Pt–CNT catalyst

Cyclic voltammetry (CV) is one of the most common techniques used in electrochemical studies in fuel cell reactions (Rajesh *et al.,* 2002; Tang *et al.*, 2004; Tang *et al*., 2004a; Li and Hsing, 2006; Saha, *et al*., 2006; Zhao *et al*., 2006; Nataranjan and Hamelin, 2007). Figures 5.11 – 5.14 show the cyclic voltammetric results for Pt–CNT catalysts as a function of Pt loading. The two ways to express the catalytic activity of a fuel cell catalyst are the mass activity and the specific activity (Zhao *et al.*, 2006). The mass activity indicates the current per unit amount of catalyst and has a more practical value in fuel cells because the cost of the electrodes depends on the amount of Pt used. On the other hand, the specific activity which measures the unit surface area of a catalyst shows the Pt electrocatalytic activity of Pt atoms on the particle surface (Rajalakshmi *et al.,* 2005; Zhao *et al.*, 2006). In this work, the CV plots have been presented with the ordinate in milliamperes per milligram of Pt.

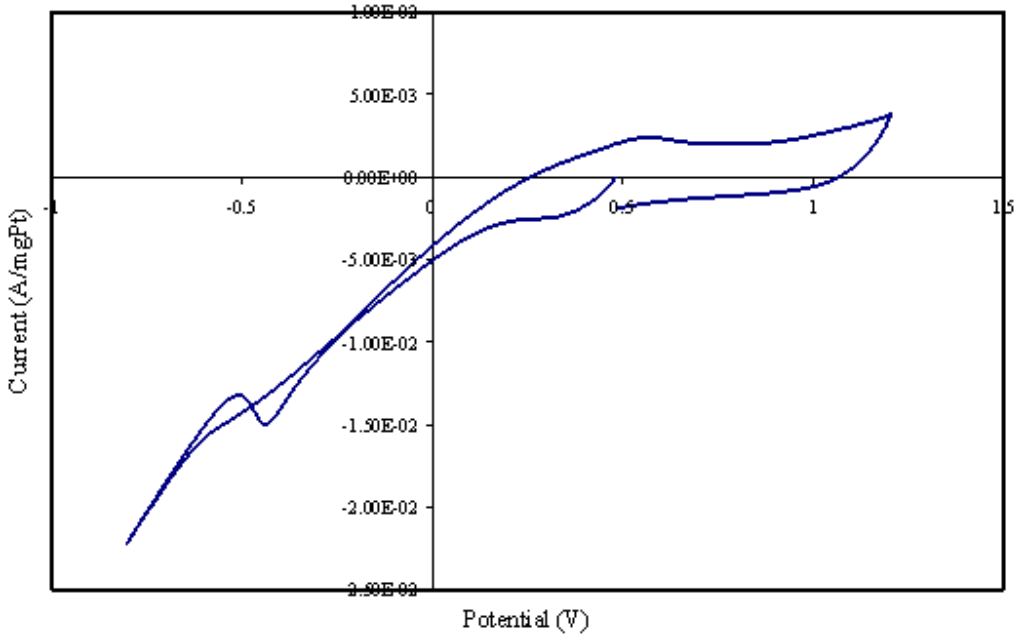

Figure 5.11: Cyclic voltammogram of 10 wt% Pt–CNT catalyst at a scan rate of 20 mV/s in nitrogen saturated 0.5 M H_2SO_4

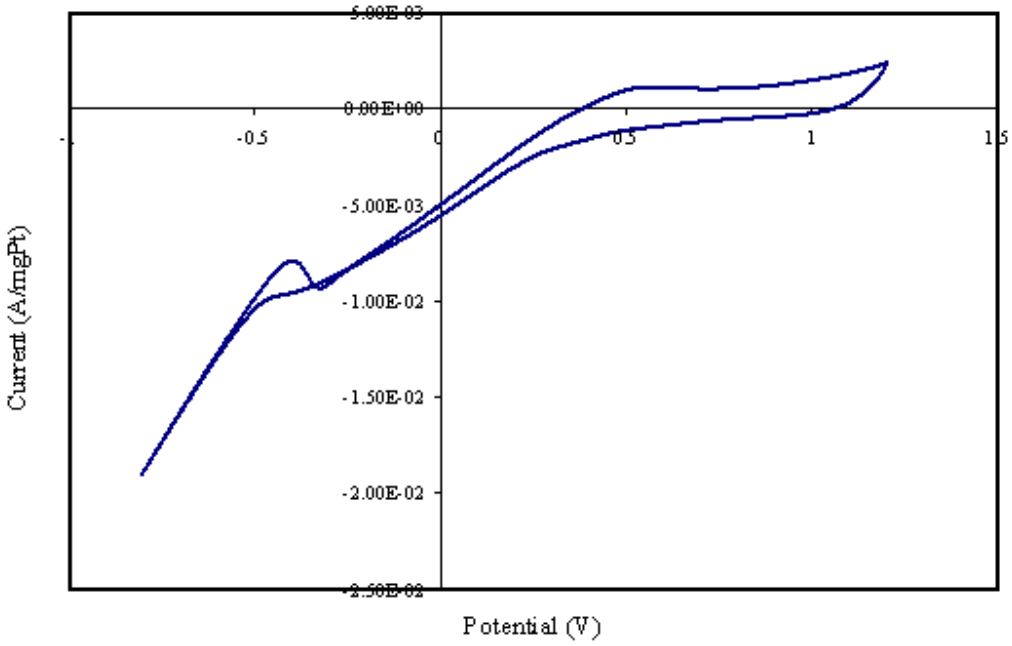

Figure 5.12: Cyclic voltammogram of 20 wt% Pt–CNT catalyst at a scan rate of 20 mV/s in nitrogen saturated 0.5 M H_2SO_4

Figures 5.11 and 5.12 show the respective electrochemical and electrocatalytic properties of 10 and 20 wt% Pt–CNT catalysts investigated in 0.5 M H_2SO_4 aqueous solution in the potential range of –1.5 and +1.5 V, using an average of five scans for each sample. It can be observed that the peak current density obtained in 20 wt% Pt–CNT is slightly greater than that in 10 wt% Pt–CNT catalyst sample. This anticipated finding is obviously due to the higher loading in the 20 wt% Pt–CNT catalyst than in 10 wt% Pt–CNT sample. A similar trend is observed in the 30 and 40 wt% Pt–CNT samples. On the other hand, it can be observed that the oxygen reduction reaction (ORR) current is noticeable in all the samples over the potential range studied. This means that all the samples have obvious electrocatalytic activity for ORR. This favourably compares to the work of Zhao *et al.* (2003), Li *et al*. (2004a), Fei *et al*. (2005), Maiyalagan *et al*. (2005), Rajalakshmi *et al*. (2005), Li *et al*. (2006), Xu and Hou, (2007) and Hernandez–Fernandez *et al*., (2008). Table 5.2 shows the peak current density (maximum current) and the corresponding voltage values for various loadings of Pt–CNT catalysts as obtained from the cyclic voltammetric results in Figures 5.11 – 5.14.

Table 5.2: Electrocatalytic activity of Pt–CNT catalysts

Catalyst loading (Pt–CNT	Maximum current (A/mgPt)	Minimum current (A/mgPt)	Maximum voltage (V)	Minimum voltage (V)
10 wt%	3.0×10^{-3}	-1.80×10^{-2}	+1.17	- 0.57
20 wt%	4.0×10^{-3}	-2.25×10^{-2}	+1.24	- 0.57
30 wt%	3.7×10^{-3}	-7.40×10^{-3}	+0.45	- 1.00
40 wt%	2.2×10^{-2}	-2.10×10^{-2}	+0.60	- 1.00

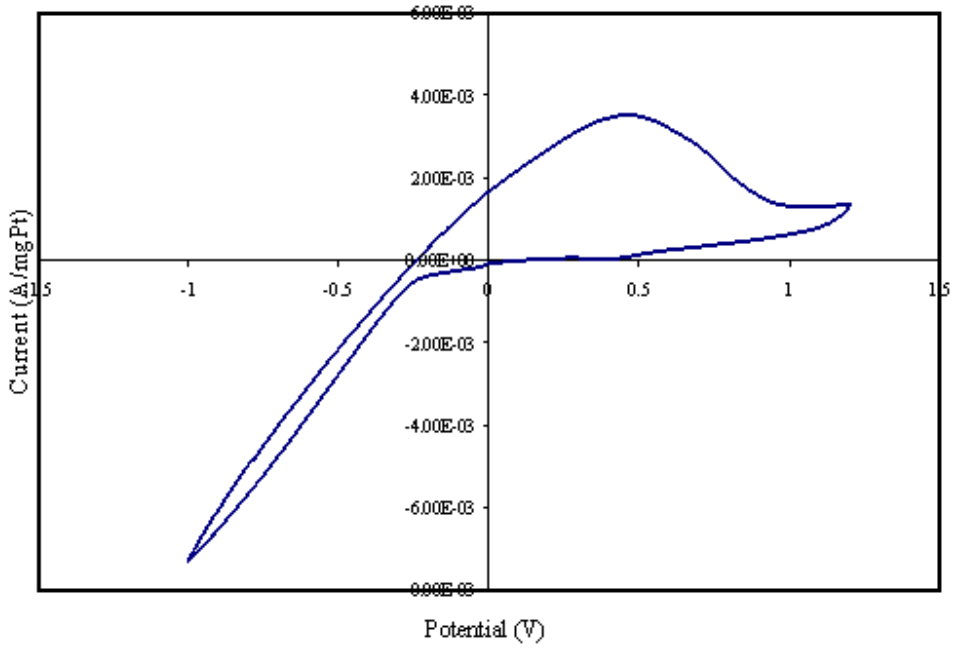

Figure 5.13: Cyclic voltammogram of 30 wt% Pt–CNT catalyst at a scan rate of 20 mV/s in nitrogen saturated 0.5 M H_2SO_4.

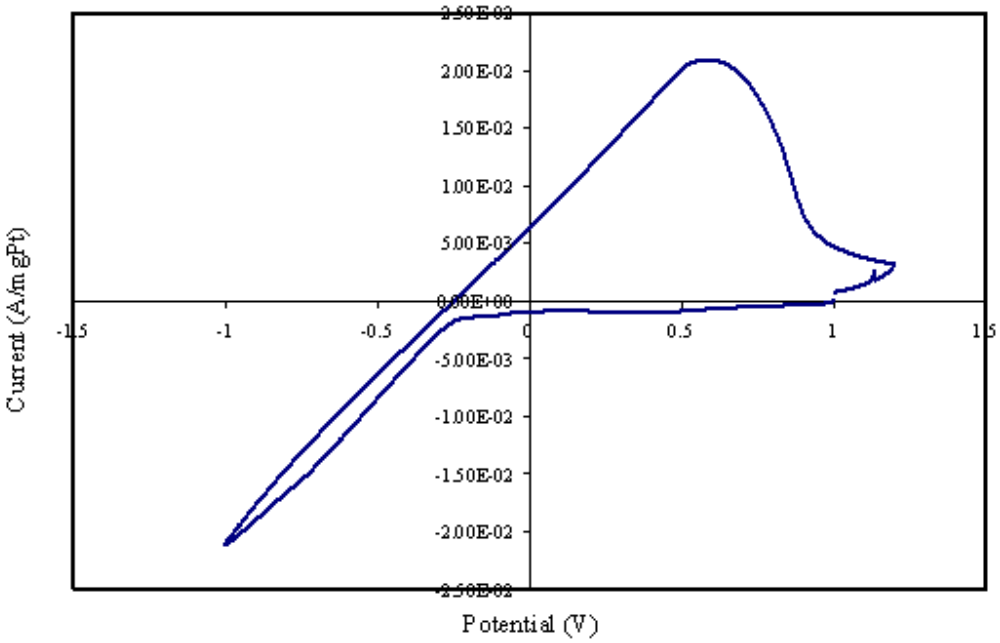

Figure 5.14: Cyclic voltammogram of 40 wt% Pt–CNT catalyst at a scan rate of 20 mV/s in nitrogen saturated 0.5 M H_2SO_4.

5.4 Analysis of the Catalyst Electrodes

Carbon fiber paper (or carbon cloth) has been used both as an effective electrode substrate and as a catalyst support in fuel cells (Wang *et al.*, 2004a; Chen *et al.*, 2005a; Golovko *et al.*, 2005; Waje *et al.*, 2005; Chen *et al*., 2006a; Tzeng *et al.*, 2006). This is due to its network–like and highly porous structure.

Figure 5.15 shows the SEM images of the carbon paper used for the preparation of catalyst electrodes in this work. It is seen that the paper is made of woven carbon fibres, which are themselves made from graphitized polysaccharide or pitch fibres (Buckley and Edie 1993; Morgan 2005). The SEM images of the carbon paper coated with catalyst ink (the electrodes) are shown in Figure 5.16.

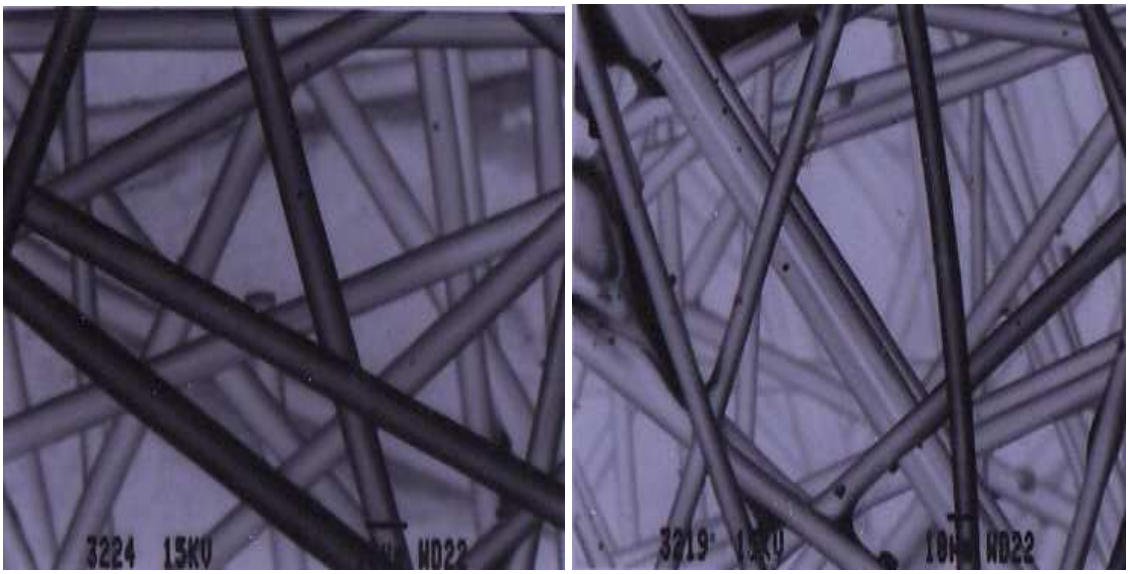

Figure 5.15: SEM images of carbon paper used in this study.

Figure 5.16 a shows the electrode with a single layer catalyst coating while Figure 5.16 b is the electrode with a double layer catalyst layer coating. The thickness of the coating determines the platinum loading on the electrodes.

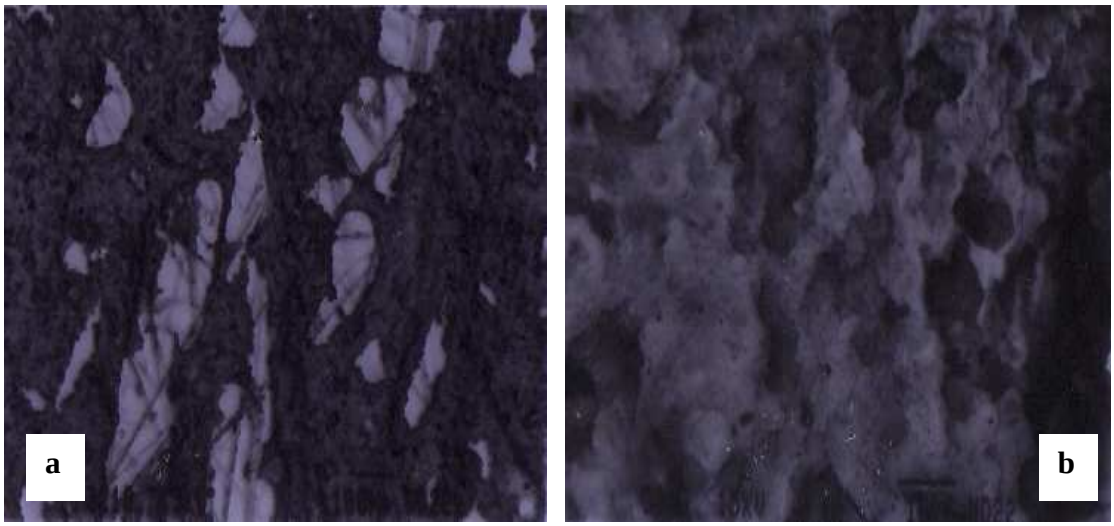

Figure 5.16: SEM images of the electrode samples

5.5 The Performance of MEA in a Single PEM Fuel Cell

A typical membrane electrode assembly used to test the performance of the electrodes has the following composition and dimensions:

Carbon paper support = 310 µm

Diffusion layer = 530 µm

Catalyst layer = 220 µm

Solid polymer electrolyte = 220 µm

The characteristics of the fabricated electrodes for a single PEM fuel cell (25 cm^2) operated at 25^oC is shown in Table 5.3.

Table 5.3: Characteristics of the fabricated electrodes

Electrode samples wt% Pt–CNT	Open circuit voltage (mV)	Power density (mW/cm^2)	Exchange current density i_o (mA/cm^2)	Tafel constant, A (mV)
10	307.45	1485.827	0.0004	46.91
20	520.48	2684.053	0.37	86.53
30	689.79	3703.929	4.35	123.33
40	718.75	4029.74	11.8	125.9

In the running of the PEM fuel cell, hydrogen fuel is oxidized at the anode while oxygen is reduced at the cathode to produce electricity, heat and water. The chemical reaction of this process is shown in equation 5.3;

$$2H_2(g) + O_2(g) = 2H_2O(l) \qquad 5.3$$

The oxygen electrode has a higher potential than the hydrogen electrode, hence oxygen is reduced to water while hydrogen is oxidized to H^+ when the two electrodes are externally connected together. The hydrogen reaction rate is directly proportional to the current, since for each hydrogen molecule that reacts, two electrons are formed.

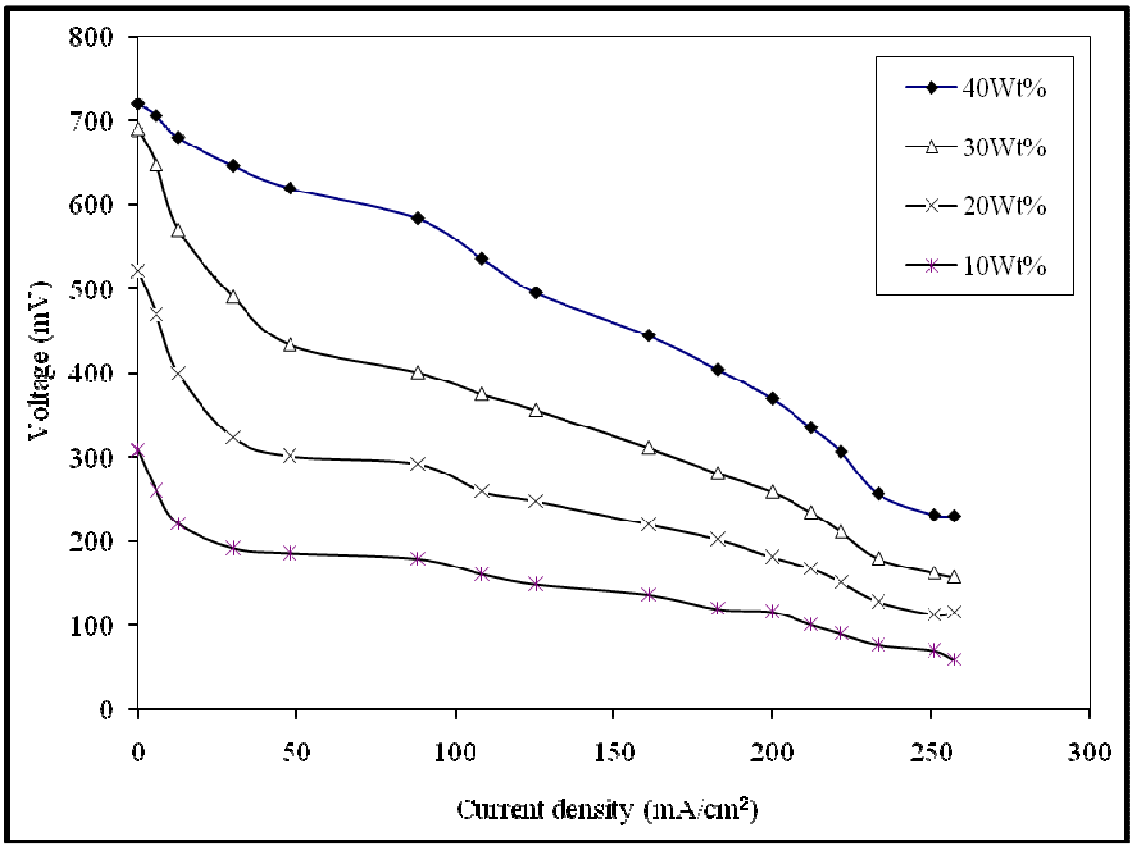

Figure 5.17: Polarisation curve of a single cell operated at 25°C with H_2:O_2 ratio of 1:2

The polarisation curve in Figure 5.17 shows the behaviour of MEAs in terms of cell potential and current density. It can be observed from the figure that higher potential and corresponding higher current densities are obtained at higher loadings of the electrode. This indicates that the performance of the electrodes increases with increase in Pt loading in the catalyst layer when made by the same fabrication process and run at the same operating conditions. This higher performance of the cell at the higher current densities of these electrodes can be attributed to the smaller particle size and lower agglomeration of the Pt particles in these catalysts (Figures 5.5 and 5.6). The relative performance of

PEM fuel cell depends strongly on the electrical conductivity of the CNT support as well as the ability of the catalyst support to transport electrons to the current collector of the MEA. The large voltage drops recorded in the polarisation curve in the region of low current densities indicates the slow kinetics of the oxygen reduction reaction at the cathode of the cell.

The power density values of the electrodes are plotted in Figure 5.18 as a function of the current density. From the figure, it is seen that the power density increases with Pt loading on the electrodes. Thus, the power density increases from 23.12 mW/cm^2 in the 10wt% electrode sample to 36.83 mW/cm^2 in 20wt% electrode sample, and from 51.58 mW/cm^2 in 30wt% to 73.68 mW/cm^2 in 40wt% electrode sample.

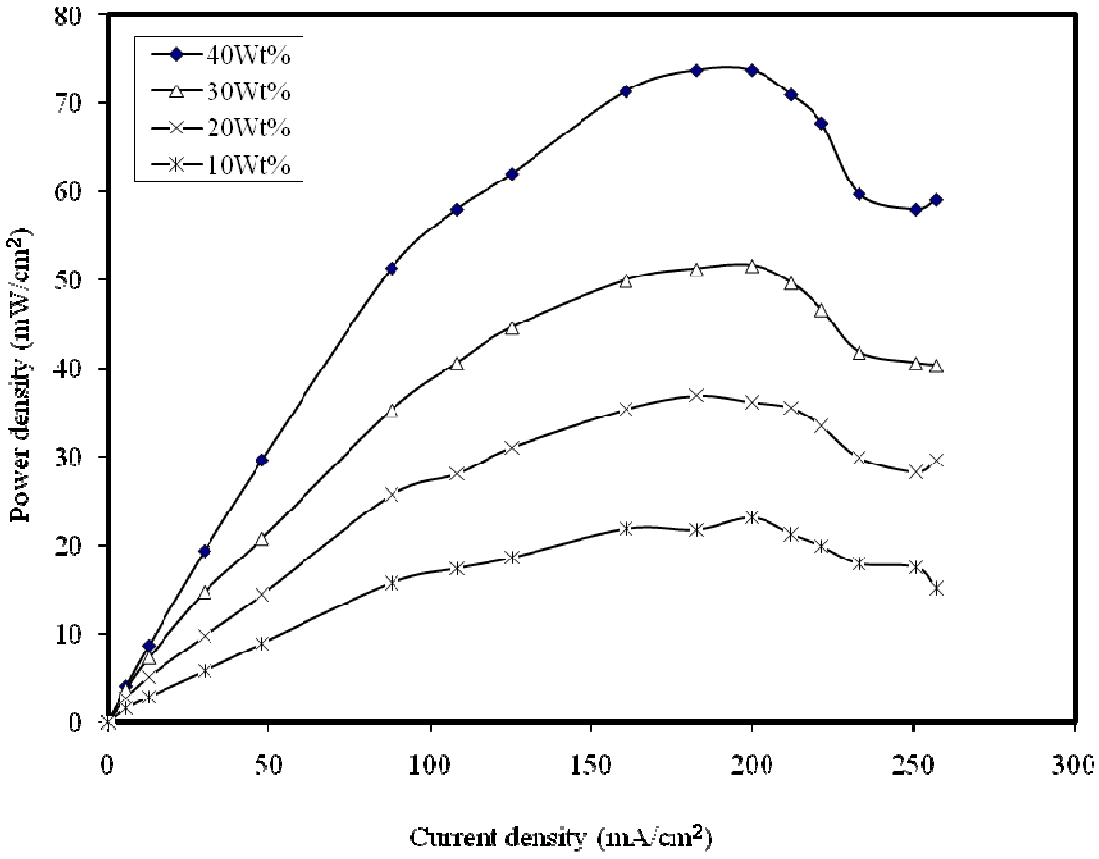

Figure 5.18: Power density Vs current density for a single cell (25 cm^2) for electrodes operated at 25°C.

The values of voltages and corresponding current densities obtained in this cell were recorded at room temperature of about 25°C. Most authors operate their cells at elevated temperature to obtain slightly higher values of voltages and current densities (Liu and Norskov, 2001; Horsfall and Lovell, 2001; Rajalakshmi *et al*., 2005; Amirinejad *et al*., 2006; Saha *et al*., 2006; Song *et al*., 2007). Figure 5.19 is an example of the comparison between the polarisation curves for Amirinejad and co-workers' (2006) single cell which was operated at 50°C with the experimental curves obtained in this work.

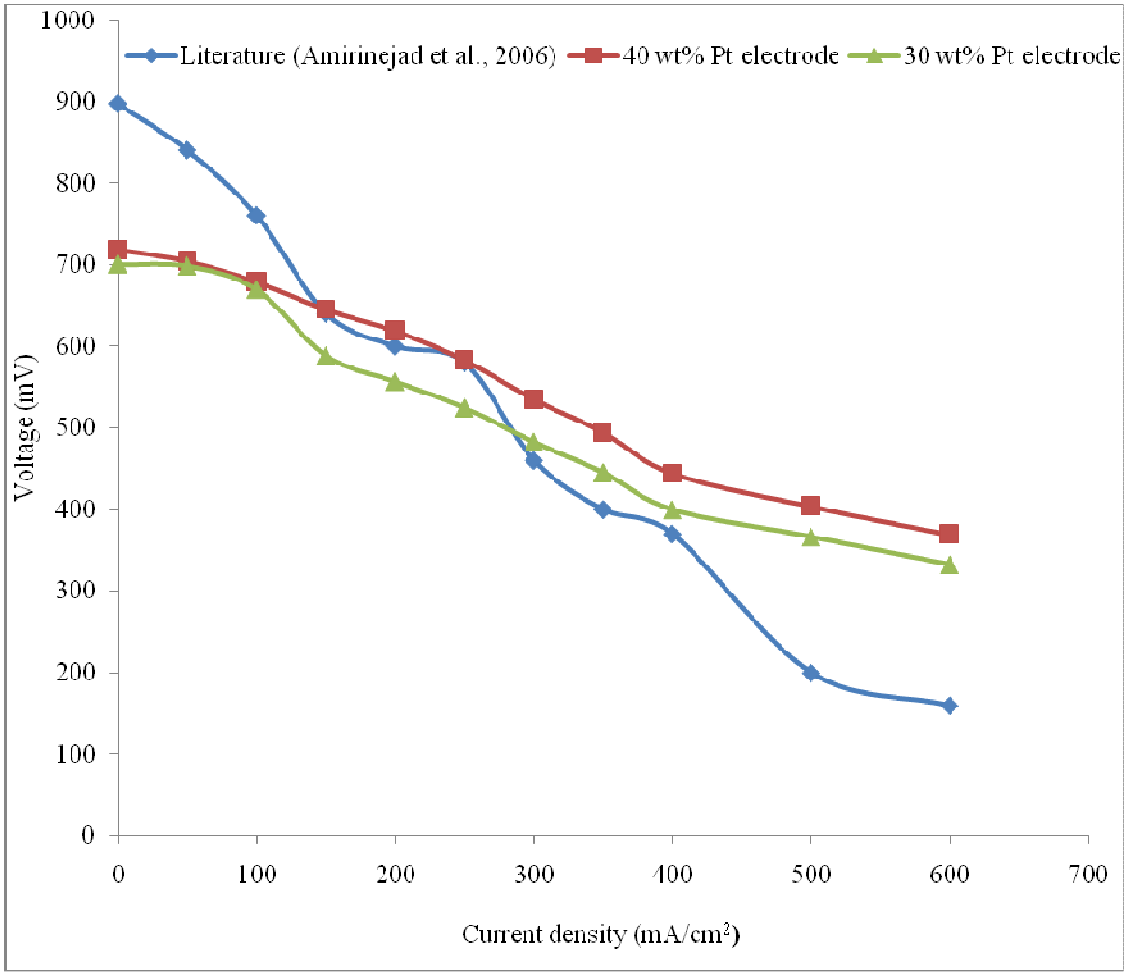

Figure 5.19: Polarisation curve showing the open voltage for experimental and literature in a single cell operated with H_2:O_2 ratio of 1:2

It is observed from the Figure that the open circuit voltage from the literature (897 mV) is slightly higher than the experimental open circuit voltages obtained (718 mV for 40 wt% Pt and 700 mV for 30 wt% Pt) in this study. This difference can be attributed to the slightly higher temperature (50°C) employed in the former study since all other

conditions of the two cells were the same. The temperature effect which affects the output of fuel cells is caused as a result of activation losses in the cell.

Activation losses which are those losses associated with the initial dramatic voltage losses in PEM fuel cells, are usually high when PEM fuels are operated at low temperatures (Rayment and Sherwin, 2003). These losses are basically representative of a loss of overall voltage at the expense of forcing the reaction to completion, which is forcing the hydrogen to split into electrons and protons, and for the protons to travel through the electrolyte, and then combine with the oxygen and returning electrons. This loss is often termed over potential, and is essentially the voltage difference between the two terminals. Therefore, it can be predicted that the performance of this cell would have been higher if operated at higher temperature since the activation loss at high temperatures is minimal. This is due to the fact that the value of exchange current density (*io*) increases almost two orders of magnitude over the span of operational temperatures used. Also increase in the operational pressure will reduce the activation losses since the higher the pressure at the cathode the quicker the reaction will be "forced" to take place (Rayment and Sherwin, 2003).

The effects of humidification of inlet gases on the fuel cell performance were not fully studied in this work, but both the anode and cathode were humidified during the reaction. The temperature of the cell was constant at $25^{o}C$ and the humidification temperature is equal to the cell temperature when humidified fuel and oxidant were used. It was

observed that low voltages and corresponding current densities were obtained when dry inlet hydrogen gas was used which indicates that humidification of the fuel gas has a considerable effect on the performance of the cell. This behaviour can be explained by the lower ionic conductivity of the membrane in dry conditions. The proton must be transferred from the anode side through the membrane to the cathode side of the cell and humidified anode side can enhance this operation. In the same vein, full hydration of the membrane is necessary to enhance its ionic conductivity and according to Abdulkareem (2009), the water uptake of the sulphonated membrane is very high and takes about 96 hours for full hydration of the membrane. This further explains why both inlet gases were humidified. The thickness of the membrane was uniform at 220 µm as conductivity is directly related to the membrane thickness (Atkins, 1987).

An attempt was made to investigate the long term testing of the MEA in the cell. This experiment could not be properly conducted due to practical constraints. However, the cell was run for 600 minutes and the result obtained is presented in Figure 5.20. From this Figure it is seen that the cell voltage decreases gradually from the open circuit voltage value of 718 mV until some stability was attained between 555 – 558 mV for about 180 minutes before it finally decreases to 438 mV after 420 minutes and this value is maintained for the final duration of the experiment.

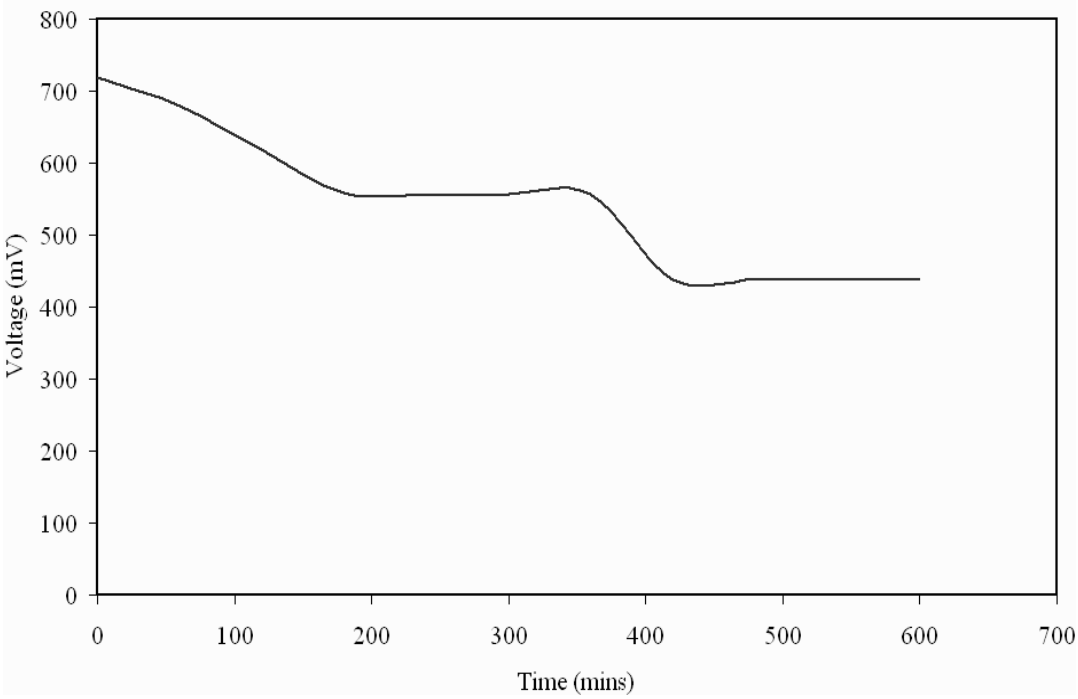

Figure 5.20: Performance durability of a single cell (25 cm^2) for electrode operated at 25^oC.

The efficiency of a PEM single cell for a particular electrode is given by Larmine and Dicks (2001) in equation 5.4 as:

$$\text{Cell efficiency } \eta = \mu f \frac{V}{1.48} \text{ X } 100 \qquad 5.4$$

where μf is called fuel utilization coefficient = $\dfrac{\text{mass of fuel reacted in cell}}{\text{mass of fuel inputed to the cell}}$

Based on the stoichiometric ratio of hydrogen to oxygen in the PEM fuel cell system, 2 moles of hydrogen are required for 1 mole of oxygen to produce 2 moles of water as

stated in equation 5.3. This is, however, not the case in the practical PEM fuel cell, as not all the hydrogen passed into the cell is completely consumed by oxygen. The exchange current density has been identified as the major parameter controlling the performance of electrons in a PEM fuel cell (Iyuke *et al*., 2003). Therefore, an increase in this parameter results in an increase in efficiency of the cell. From Table 5.3**,** it can be observed that the values of the exchange current density increase with increase in Pt loading on the catalyst. In other words, the electrode efficiency decreases: 40wt% < 30wt% < 20wt% < 10wt%.

5.5.1 Kinetics of the PEM fuel cell

In fuel cells, the overvoltage, ΔV, due to kinetics of the reaction is a function of the current density (which is directly proportional to the rate of reaction) and is often described by the Tafel equation given in equation (5.5) as;

$$\Delta V = A \ln \frac{i}{io} \qquad 5.5$$

where, A is the Tafel constant (Volts), i_o is the exchange current density (mA/cm^2), which is the value on the Tafel plot when the current begins to move away from zero.

The Tafel equation was therefore used to model and predict the voltage of this PEM fuel cell system at room temperature of about 25^oC. The theoretical maximum voltage of most fuel cells is usually taken as 1200 mV. This is called the “open circuit voltage”. In this

cell, the open circuit voltage is 718 mV and any deviation from this maximum value is termed overvoltage. This deviation allows useful statements to be made about the kinetics of the fuel cell reactions. For every cell system there is a critical current called the "exchange current density" (i_o). When the current densities $i < i_{o,}$ the cell voltage is equal to the theoretical value and for current densities $i < i_{o,}$ there is a rapid fall in cell voltage, due to a slow reaction rate constant (kinetics). Therefore, it is important to have as high a value of i_o as possible, and as rapid kinetics as possible.

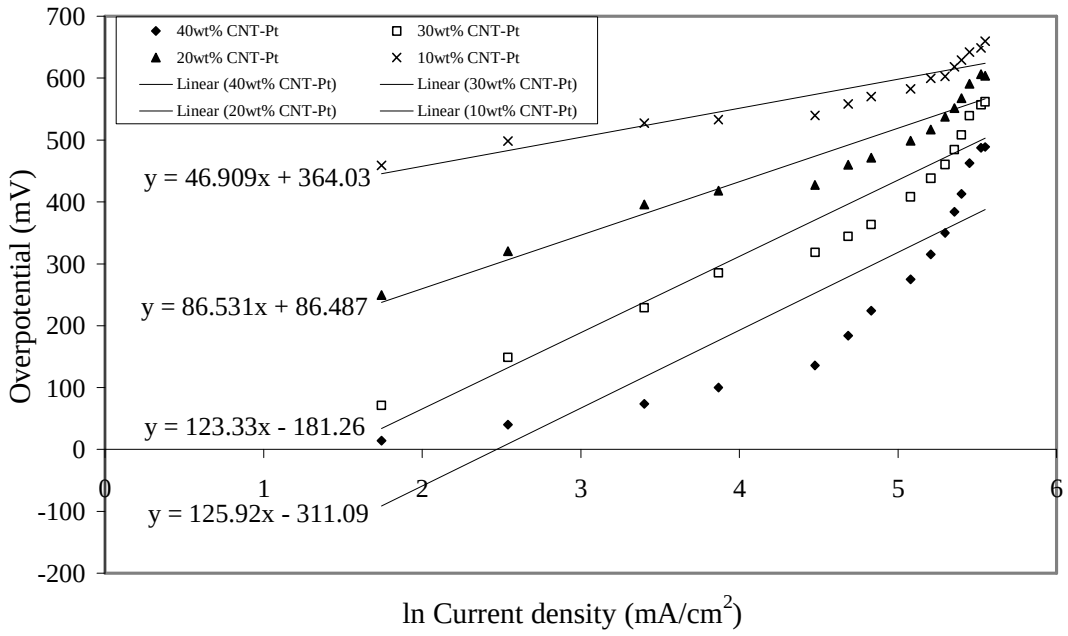

Figure 5.21: Tafel plot for overpotential of a single cell operated at 25°C

Figure 5.21 shows the Tafel plot obtained from the polarisation curve of the MEA fabricated with varying Pt loading on the electrodes. The best–fit lines of the points obtained from the Figure are stated in (5.6 – 5.9) as;

For 40wt% catalyst electrode: y = 125.92x – 311.09 5.6

For 30wt% catalyst electrode: y = 123.33x – 181.26 5.7

For 20wt% catalyst electrode: y = 86.53x + 86.49 5.8

For10wt% catalyst electrode: y = 46.91x + 364.03 5.9

From the Tafel plot in Figure 5.21, using the open circuit voltage of 718 mV obtained during the experiment (and not the theoretical value of 1200 mV), it is observed that an MEA fabricated with 30 and 40 wt% catalyst electrodes obeys the Tafel equation. This is due to the fact that the Tafel equation is not obeyed at high values of overvoltage (Keith, 2008). Therefore the two catalysts that obey the Tafel equation are suitable to model the performance of the catalyst electrode in the cell.

Using the Tafel equation, $\Delta V = A \ln \frac{i}{io}$ 5.5

which can be transformed to the form in (5.10)

$\Delta V = A\ln i - A\ln i_o$ 5.10

Comparing equation 5.10 with the linear equation obtained in polarisation plot of 40wt% catalyst in Figure 5.17, (i.e. equation 5.6) gives;

$\Delta V = A\ln i - A\ln i_o$ 5.10

y = 125.9x – 311 5.6

Equation 5.6 can be re written as 5.11

$\Delta V = A\ln i - A\ln i_o$ 5.10

$\Delta V = 125.9\ln i - 311$ 5.11

Solving the two equations 5.10 and 5.11 above yields *A* value equal to the slope of equation 5.11 and equation obtained in MEA fabricated with 40wt% catalyst electrode.

Therefore,

$A = 125.9$ mV (0.1259 V)

To solve for i_o, the intercept of equation 5.10 is equal to $-A\ln i_o$, so that

$A\ln i_o = 311$,

$125.9 \ln i_o = 311$, so that $\ln i_o = \frac{311}{125.9} = 2.4702$

$i_o = 11.8$ mA/cm^2

Substituting the values of A and *io* in equation 5.10 gives;

$\Delta V = 125.9 (\ln \frac{i}{12.04})$ or

$\Delta V = 125.9 \ln i - 125.9 \ln i_o$ 5.12

Therefore, equation 5.12 can be used to model the performance of 40wt% catalyst electrode used in the cell, while the cell voltage can be obtained from the overpotential value of the electrode. Thus:

Voltage of the cell (V) = Open circuit voltage (Vocv) – Overvoltage (ΔV) 5.13

i.e. V = Vocv – Aln i – Aln i_o 5.14

Equation 5.14 above is used to simulate the performance of this electrode and the result is compared with experimental voltage as shown in Figure 5.22.

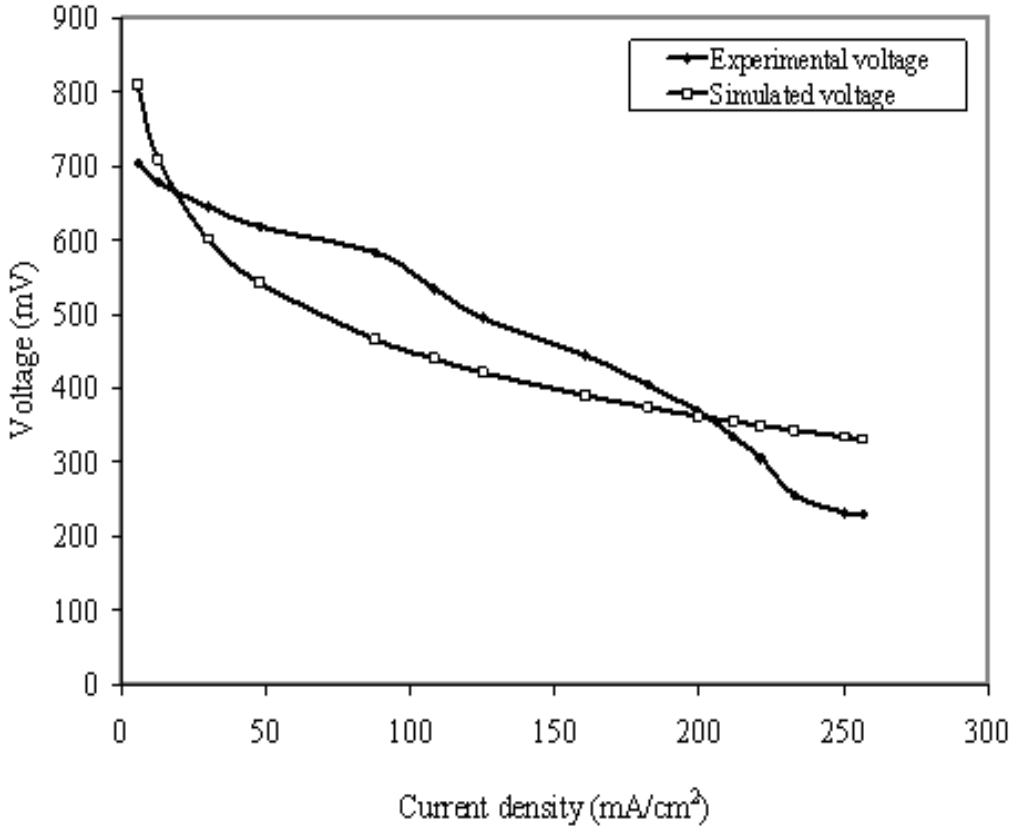

Figure 5.22: Experimental and simulated polarization of 40wt% Pt catalyst electrode.

It is noted that the deviation of the voltage from ideal value of 1200 mV is fairly high when compared to the values measured in the laboratory. This is suspected to be due to Ohmic losses within the cell, which might have been caused during MEA fabrication.

The cell voltage can also be calculated by using the Hirschenhofer *et al.*, (1994) expression as stated in equation 5.15.

$$V_e\left(T,\ p,\ p_{o_2},\phi\right)=V_o\left(T,\ p,\ p_{o_2},\phi\right)_e - b\left(T,\ p,\ p_{o_2},\phi\right)\log\left(i_e\right) - R\left(T,\ p,\ p_{o_2},\phi\right)i_e - m\left(T,\ p,\ p_{o_2},\phi\right)\exp\left[n\left(T,\ p,\ p_{o_2},\phi\right)i_e\right] - b\left(T,\ p,\ p_{o_2},\phi\right)\log\left[\frac{p}{p_{o_2}}\right] \quad (5.15)$$

where; Ve = cell voltage (mV), T = temperature (^oC), P = total pressure (kPa), P_{O2} = partial pressure of oxygen (kPa), Vo = open circuit voltage (mV), b = Tafel constant (mV), i_o = current density (mA/cm^2), and R = membrane resistance (Ohm/cm^2), m = fitting constant which is taken as flooding constant of the cell and n = oxygen concentration (mol/dm^3).

Equation 5.15 provides more accurate information on the cell voltage since it incorporates the inefficiencies of the activation polarization, Ohmic polarization, and the concentration polarization. The constants: Vo, b, R, m and n, depend on the type of MEA, the type of oxidant, and the local pressure, temperature, humidity and oxygen concentration for the elemental unit. The simplified form of equation 5.15 can be written as:

$$\text{Vcell} = \text{Vo} - \text{blog}i_o - \text{R}i_o - \text{m expn}\ i_o - \log\frac{\text{P}}{\text{PO2}} \quad (5.16)$$

where Vcell is the simulated cell voltage, b = Tafel constant, R = resistance of the membrane, P = total pressure (kPa) and P_{O2} = partial pressure of oxygen (kPa). The

fitting constant has an exponential relationship with the current density (Appendix V), i.e. $m = 193.4 \exp^{-13.9io}$ and the resistance of the membrane, R = 0.57344 Ωcm^2 (Abdulkareem, 2009 and Idibie, 2009). The cell performance in relative to the electrode is modelled by substituting the cell data for 40wt% Pt catalyst electrode in the equation 5.16 and the results obtained (Appendix V) were compared with the experimental voltage as shown in Figure 5.23.

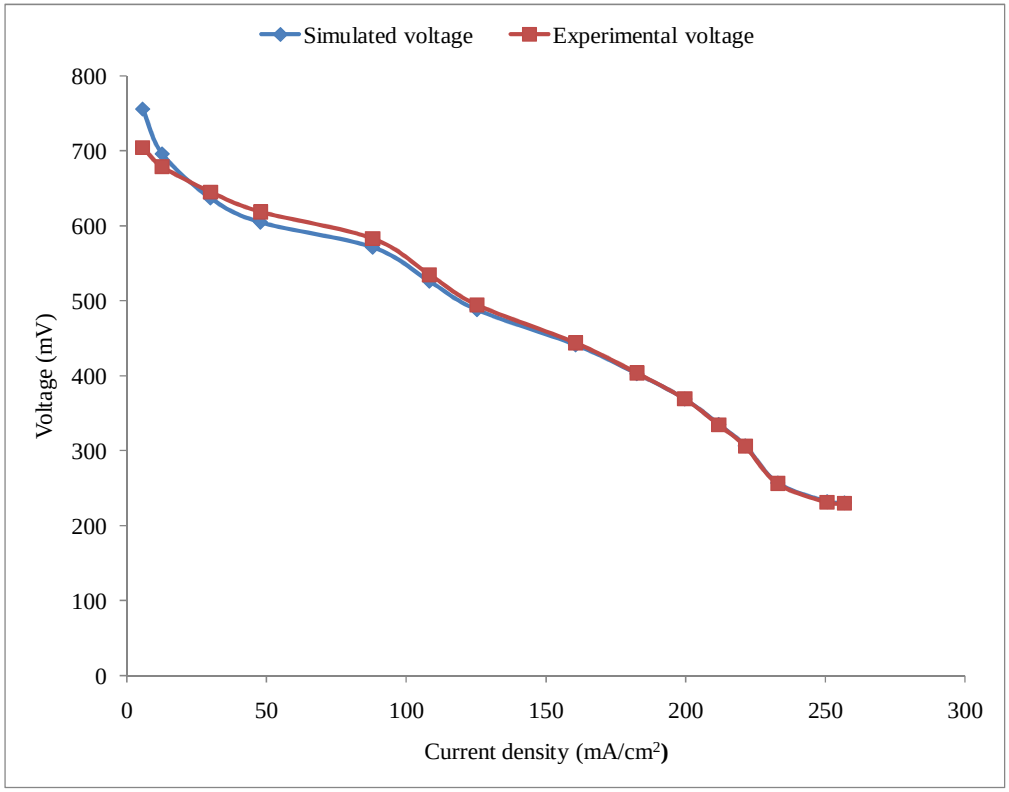

Figure 5.23: Hirschenhofer's model of voltage of 40wt% Pt catalyst electrode.

It is seen from Figure 5.23 that the equation 5.16 gives a good model of the performance of the 40 wt% Pt catalyst electrode in the cell with correlation factor, R^2 = 0.996. This

model good conformity can be attributed to other depending factors which were incorporated in the model. This is in contrast to the performance obtained in the Tafel model (Figure 5.22) in which conditions such as Ohmic resistance and activation polarization are not incorporated in the model.